

## Effects of Sintering Atmosphere on The Optical, Thermal and Electrical Properties of Inkjet Printed $Zn_xCu_{(1-x)}Fe_2O_4$ Thin Films

Lim Joon Hoong<sup>1,\*</sup>

<sup>1</sup> School of Computer Science and Engineering, Taylor's University Lakeside Campus, 47500 Subang Jaya, Malaysia

### ARTICLE INFO

#### Article history:

Received 2 September 2020  
Received in revised form 4 February 2021  
Accepted 15 February 2021  
Available online 21 March 2021

#### Keywords:

Thin film; Sintering atmosphere; Zinc copper ferrite; Thermoelectric properties

### ABSTRACT

The effects of sintering atmosphere on the optical, thermal, and electrical properties of inkjet-printed  $Zn_xCu_{(1-x)}Fe_2O_4$  thin films have been investigated. The thin film samples were sintered separately in vacuum and oxygen. The obtained samples were then characterized by X-ray diffraction (XRD), optical band gap, electrical conductivity, Seebeck coefficient, and thermal conductivity. XRD analysis showed that the fabricated samples have a cubic spinel structure of zinc copper ferrite regardless of the sintering atmosphere. The electrical conductivity of  $Zn_xCu_{(1-x)}Fe_2O_4$  thin films sintered in oxygen was about 5 % higher compared to  $Zn_xCu_{(1-x)}Fe_2O_4$  thin films sintered in vacuum. The optical band gap shows that the samples sintered in oxygen had a smaller bandgap compared to samples sintered in vacuum. The electronic band structure simulated through ABINIT shows  $Zn_xCu_{(1-x)}Fe_2O_4$  is an indirect band gap material. A smaller electronic bandgap was observed in O<sub>2</sub> rich condition and was in agreement with the optical band gap and electrical conductivity test results. The Seebeck coefficient of  $Zn_xCu_{(1-x)}Fe_2O_4$  thin films sintered in oxygen remained positive, confirming charge transport by hole carriers as p-type semiconductors. A change from p-type to n-type semiconductors was observed when  $Zn_xCu_{(1-x)}Fe_2O_4$  thin films sintered in vacuum.

## 1. Introduction

Thin film is a material that formed with a thickness in the range of micrometer or less [1]. Various applications such as hard coatings wear resistant films and optical devices are possible due to the unique properties of thin films [2, 3]. Thin films have become a major influence in the electronics industry due to the advantages of thin films in the reduction of dimensions [4]. Thin-film deposition techniques are broadly divided into physical and chemical methods. The physical methods commonly employ costly equipment and vacuum systems such as pulsed laser deposition and electron beam evaporation [5, 6]. Chemical methods commonly involve solution deposition onto substrates. The high cost of fabrication is one of the main drawbacks for thin-film development. This paper attempts to solve the issue by using commonly available inkjet printers to fabricate a thin film of zinc substituted copper ferrites ( $Zn_xCu_{(1-x)}Fe_2O_4$ ).

\* Corresponding author.

E-mail address: [jhlim07@gmail.com](mailto:jhlim07@gmail.com)

<https://doi.org/10.37934/arfmts.81.2.2535>

Zinc substituted copper ferrite is widely used for various applications such as radio frequency coils, transformers cores, rod antennas, and magnetic cores of read-write heads [7-9]. The properties of  $Zn_xCu_{(1-x)}Fe_2O_4$  may vary depending on the concentration of Cu and Zn in the ferrites [10]. The possibility of mixed ferrite with different composition becomes attractive. Thin films of spinel ferrites  $MFe_2O_4$  ( $M = Mn, Cu, Zn, Ni, Co, Cd, \text{etc.}$ ) exhibit excellent chemical stability and high corrosion resistivity and seem to be applicable as recording media and microwave absorbing layers [11]. Sutka [12] studied the electrical properties of Ni-Zn ferrite thin films deposited using spray pyrolysis. The conductivity of Ni-Zn ferrite films was decreased by a rising Zn content. The conductivity decreases with the increase of Zn concentration and decrease of the Ni content in a mixed system due to electron-hole compensation. Desai *et al.*, [13] performed the deposition of copper ferrite thin films by rf sputtering on fused quartz and silicon (111) substrates at temperatures ranging from 100 °C to 800 °C with slow cooling. They reported that the phase formation of as-deposited  $CuFe_2O_4$  thin films strictly depends on the annealing temperature and cooling rate. In this paper, inkjet printing was used to deposit  $Zn_xCu_{(1-x)}Fe_2O_4$  thin films.

The magnetic, dielectric, and elastic properties of mixed Cu–Zn ferrites have been studied by various researchers. Manikandan *et al.*, synthesized Cu–Zn ferrites ( $Zn_xCu_{(1-x)}Fe_2O_4$  ( $x = 0.0, 0.1, 0.2, 0.3, 0.4$  and  $0.5$ )) by microwave combustion method and studied their optical and magnetic characteristics [14]. Sintering in different atmospheres such as air, vacuum, oxygen, and hydrogen may affect the electrical properties [8]. Stankiewicz *et al.*, [15] reported the effect of oxygen on the conduction of Indium oxide ( $In_2O_3$ ). The p-n junctions of  $In_2O_3$  thin films were confirmed by the sign of Seebeck coefficient at room temperature. It was observed a change in n-type to p-type of conductivity when synthesized under oxygen-rich conditions. The structural, magnetic, and optical properties of Zn-Cu ferrites have been widely reported [9] but the information regarding the thermal and electric properties of Zn-Cu ferrite is scarce. There are very few reports on the relationship between the processing method and thermoelectric properties of  $Zn_xCu_{(1-x)}Fe_2O_4$  in the literature. Besides, the main drawback of oxide materials is low electrical conductivity. This study attempts to address this issue by determining the effect of the processing atmosphere on the electrical properties. In this paper, the effect of sintering atmospheres on the thermal and electrical properties  $Zn_xCu_{(1-x)}Fe_2O_4$  thin films prepared through inkjet printing were studied.

## 2. Methodology

The thin films were prepared by inkjet printing using a desktop inkjet printer (Canon iP4870). Appropriate amounts of analytical grade  $Cu(NO_3)_2$ ,  $Zn(NO_3)_2$  and  $Fe(NO_3)_3$  were used to prepare solutions based on the ratios of  $Zn_xCu_{(1-x)}Fe_2O_4$  ( $x = 0.0, 0.2, 0.4, 0.6, 0.8, 1.0$ ). The solutions of  $Zn(NO_3)_2$ ,  $Al(NO_3)_3$ , and  $Fe(NO_3)_3$  were mixed with appropriate ratios and injected into the empty ink cartridges for printing. Repeated printings with the test solutions were used to clean the inkjet print head before printing out the test patterns. The solution usage was determined by measuring the weight of the cartridge after every 5 print cycles and varying the printed colors. The thin films were printed onto glass substrates and several repeated print cycles were required to obtain visually homogeneous films. The deposited thin films underwent thermal treatment separately in oxygen inside LT Tube Furnace HTF-14/200-60 and in vacuum inside vacuum furnace at temperature 400 °C for 4 hours. The thermal treatment was used to decompose the nitrate into oxide materials. The thin films were then characterized.

Elemental analysis of the inkjet-printed thin films was carried out using a scanning electron microscopy (SEM JEOL JSM-6460 LA Jeol Japan) equipped with energy-dispersive X-ray spectroscopy (EDX). The transmittance spectra of the films in the spectral range 200-900 nm were recorded using

a UV-Vis Spectrophotometer (Perkin Elmer LAMBDA 25). The phase analysis was carried out by X-ray diffraction (XRD Shimadzu 2000) with a Cu-K $\alpha$  radiation source ( $\lambda = 1.5418 \text{ \AA}$ ) from  $20^\circ$  to  $100^\circ$  and a  $2^\circ/\text{min}$  scan rate. Electrical conductivity was measured by using a Keithley source measure unit (Keithley Model SMU 236) based on ASTM F42-02. The thermal conductivity was measured at room temperature according to ASTM C177-13. The Seebeck coefficient measurement was carried out through a differential method at room temperature [16]. The band structure of the samples was calculated using the ABINIT program that is based on the density functional theory (DFT) Kohn-Sham equations [17].

### 3. Results

#### 3.1 Inkjet Printing

Figure 1 shows the optical morphology of the inkjet-printed thin films with subsequent print cycles. The surface change of the printed film was shown with increasing print cycles from 30 to 50 times. It can be observed that discontinuous films with gaps in between the films were formed after increasing print cycles. The gaps between the discontinuous films were getting narrower when the subsequent print cycles increased to 30 times. The uniformity of the film was observed clearly as the print cycles increased. Homogenous film was obtained with a minimum of 50 print cycles as shown in Figure 1(c). No visible change was observed in the number of print cycles was increased beyond 50. A similar trend was observed for all inkjet printing thin films. Figure 2 shows the cross-sectional image of inkjet printing  $\text{Zn}_x\text{Cu}_{(1-x)}\text{Fe}_2\text{O}_4$  ( $x = 0.6$ ) thin films. The thickness of the inkjet-printed thin film observed from the SEM was approximately  $9 \mu\text{m}$ . The  $\text{Zn}_x\text{Cu}_{(1-x)}\text{Fe}_2\text{O}_4$  thin film was successfully deposited onto a glass substrate using the inkjet printing method with several cycles of repeated printing.

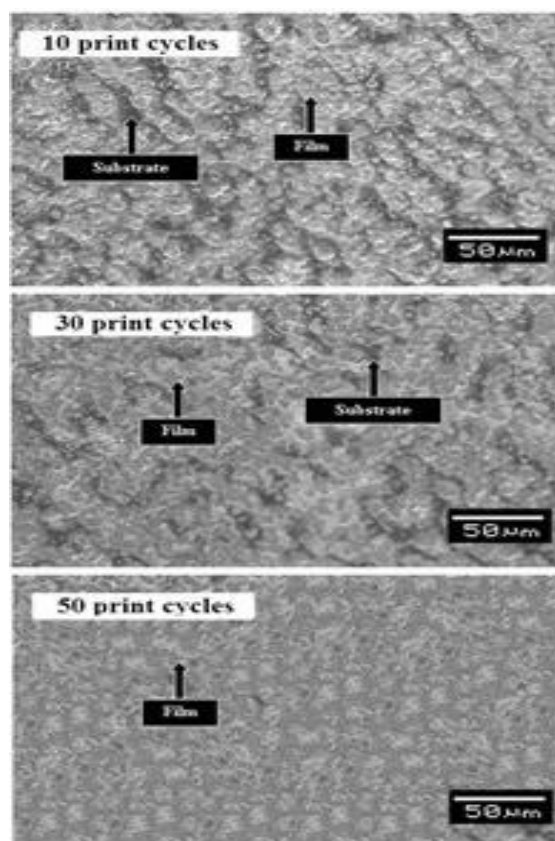
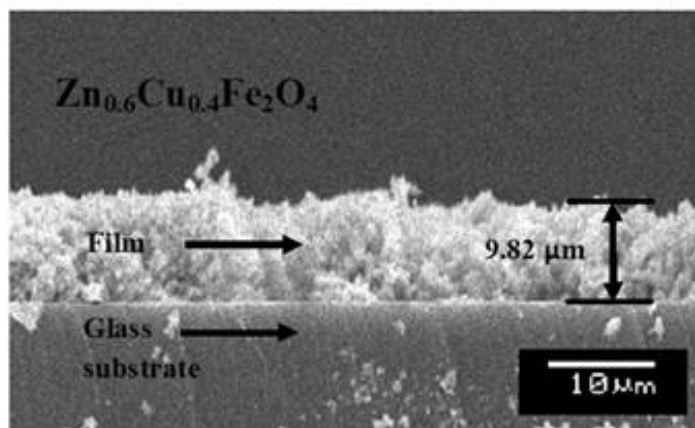


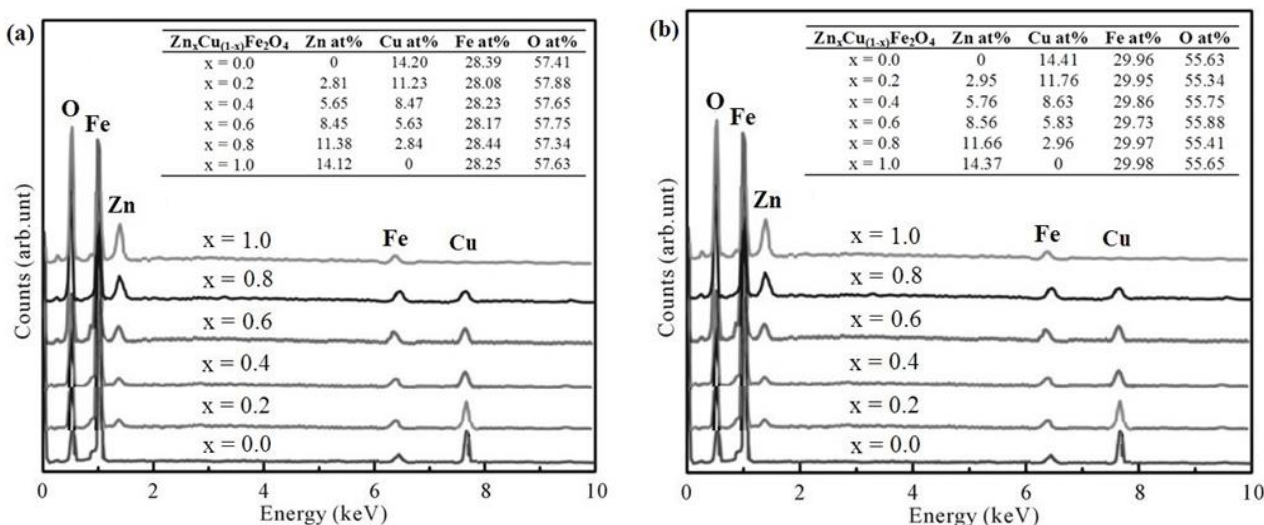
Fig. 1. Surface profile of inkjet printed thin film



**Fig. 2.** SEM image of inkjet printed  $Zn_{0.6}Cu_{0.4}Fe_2O_4$  thin film

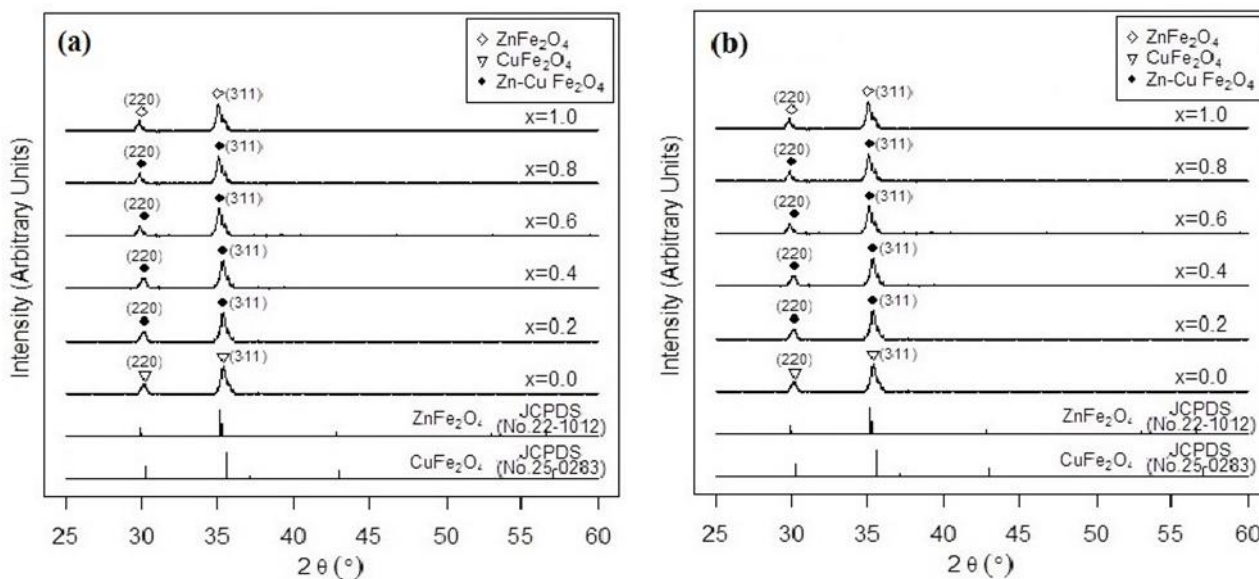
### 3.2 Composition and Phase Analysis

Figure 3 shows the elemental composition of  $Zn_xCu_{(1-x)}Fe_2O_4$  thin films sintered in oxygen and vacuum. For all  $Zn_xCu_{(1-x)}Fe_2O_4$  thin films, their EDX spectra show the presence of Zn, Cu, Fe, and O elements. The Zn signals detected in the EDX spectra increases with increasing Zn content. The inset of Figure 3(a) and Figure 3(b) shows the detailed ratios of  $Zn_xCu_{(1-x)}Fe_2O_4$  thin films ( $x = 0.0, 0.2, 0.4, 0.6, 0.8, 1.0$ ) which indicate the average Zn concentrations were close to the compositions in the precursor solutions.



**Fig. 3.** EDX spectra of  $Zn_xCu_{(1-x)}Fe_2O_4$  thin films sintered in (a) oxygen and (b) vacuum

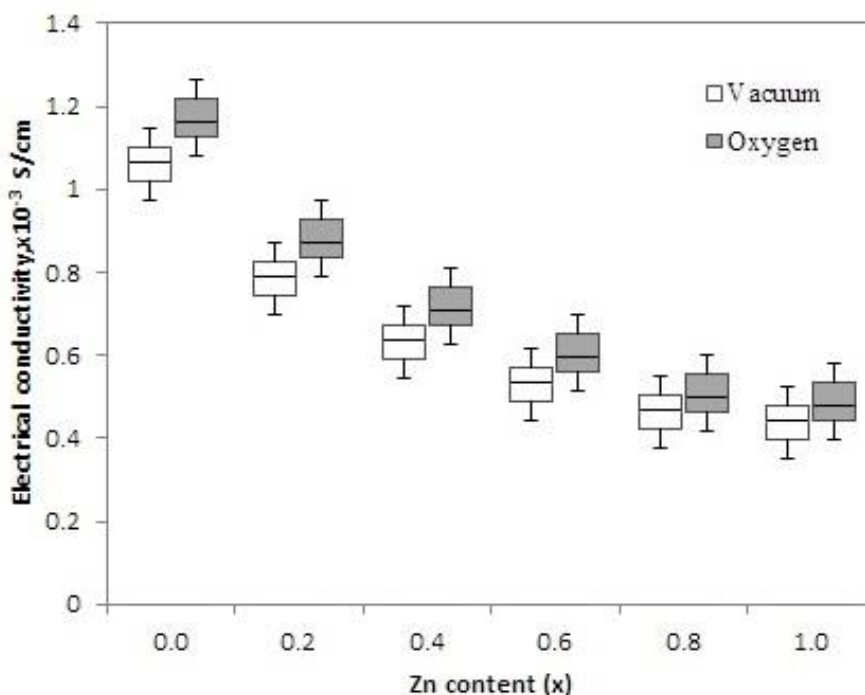
Figure 4 shows the XRD pattern of  $Zn_xCu_{(1-x)}Fe_2O_4$  thin films sintered in oxygen and vacuum. The sample peaks were identified as the plane reflection of the cubic spinel phase based on the JCPDS data file  $ZnFe_2O_4$  (No. 22-1012) and  $CuFe_2O_4$  (No.25-0283). Fewer XRD peaks were detected for thin film samples probably due to the low dimensions and crystallinity of thin films [18, 19]. There was no significant change to the crystal structure with different sintering atmospheres.



**Fig. 4.** XRD pattern of Zn<sub>x</sub>Cu<sub>(1-x)</sub>Fe<sub>2</sub>O<sub>4</sub> thin films sintered in (a) oxygen and (b) vacuum

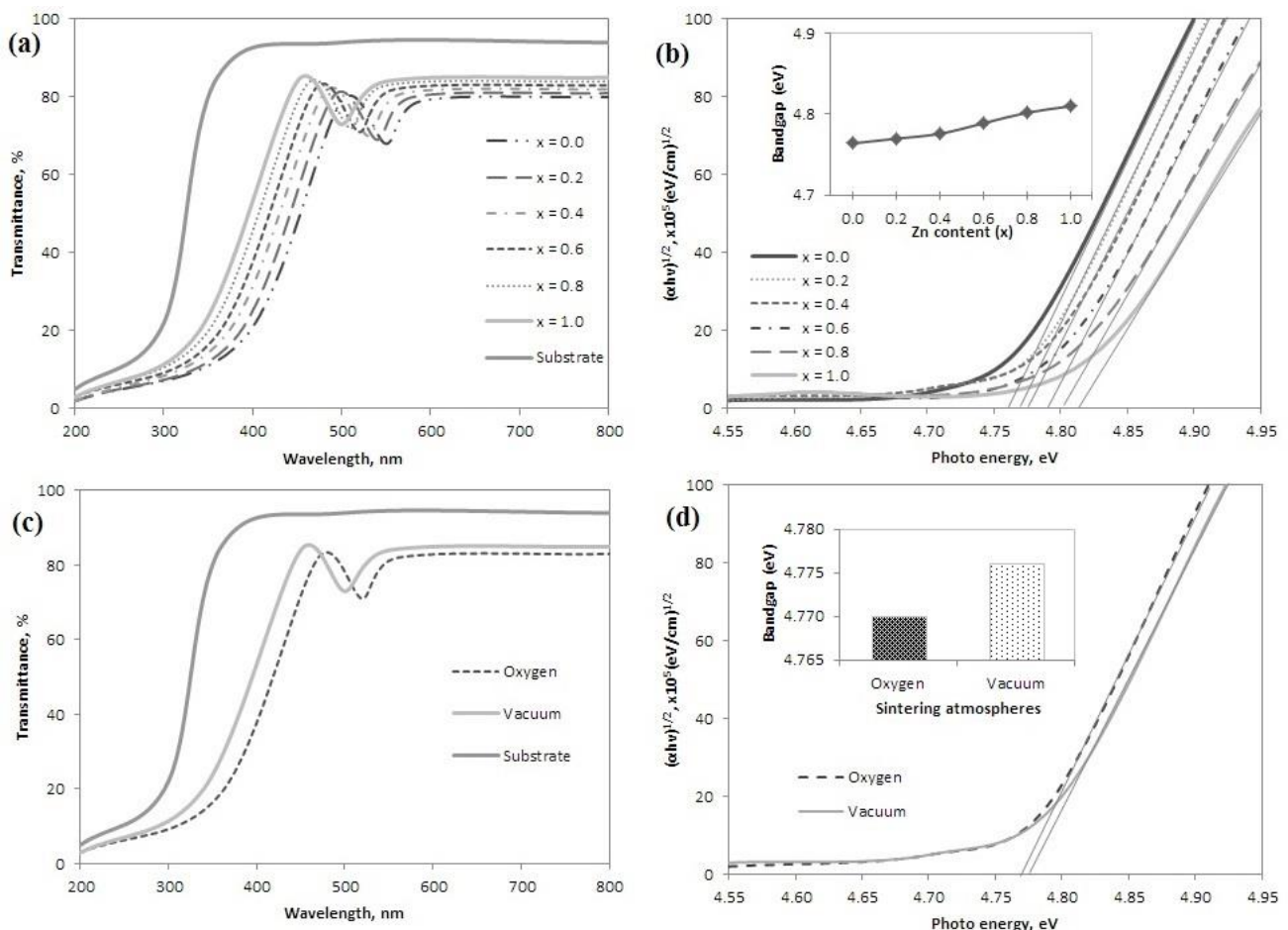
### 3.3 Electrical and Optical Analysis

Figure 5 shows the electrical conductivity of Zn<sub>x</sub>Cu<sub>(1-x)</sub>Fe<sub>2</sub>O<sub>4</sub> thin films sintered in oxygen and vacuum. The electrical conductivity of Zn<sub>x</sub>Cu<sub>(1-x)</sub>Fe<sub>2</sub>O<sub>4</sub> thin films decreased with increasing Zn content. The electrical conductivity of Zn<sub>x</sub>Cu<sub>(1-x)</sub>Fe<sub>2</sub>O<sub>4</sub> decreased might be due to the decrease of Cu with the addition of Zn. The conduction mechanism in Zn<sub>x</sub>Cu<sub>(1-x)</sub>Fe<sub>2</sub>O<sub>4</sub> was due to the interaction between Cu<sup>+</sup>-Cu<sup>2+</sup> and Fe<sup>2+</sup>-Fe<sup>3+</sup> [20]. The electrical conductivity of Zn<sub>x</sub>Cu<sub>(1-x)</sub>Fe<sub>2</sub>O<sub>4</sub> (x=0.0) thin films sintered in oxygen had the higher values (1.185x10<sup>-3</sup> S/cm). The electrical conductivity of Zn<sub>x</sub>Cu<sub>(1-x)</sub>Fe<sub>2</sub>O<sub>4</sub> thin films sintered in oxygen was about 5% higher compared to thin films sintered in vacuum. This might be due to an increase in Fe<sup>3+</sup> and Cu<sup>+</sup> brought about by the presence of oxygen [21].



**Fig. 5.** Electrical conductivity of Zn<sub>x</sub>Cu<sub>(1-x)</sub>Fe<sub>2</sub>O<sub>4</sub> thin films

Figure 6(a) shows the transmission spectra of  $Zn_xCu_{(1-x)}Fe_2O_4$  thin films recorded in the 200 to 800 nm wavelength range. The average transmittance value for the inkjet-printed  $Zn_xCu_{(1-x)}Fe_2O_4$  thin films were above 80%. The transmittance of  $Zn_xCu_{(1-x)}Fe_2O_4$  thin films increased with increasing Zn content. Figure 6(b) shows the variation of  $(\alpha hv)^{1/2}$  as a function of photon energy ( $hv$ ). The optical band gap energy for  $Zn_xCu_{(1-x)}Fe_2O_4$  ( $x = 1.0$ ) thin films was determined to be 4.81 eV. The observed optical band gap values are consistent with values reported by other researchers [22]. The inset in Figure 6(b) shows the value of optical band gap energies for  $Zn_xCu_{(1-x)}Fe_2O_4$  thin films, which increased from 4.76 eV ( $x = 0.0$ ) to 4.81 eV ( $x = 1.0$ ) as the Zn content increased. The increase in optical band gap for  $Zn_xCu_{(1-x)}Fe_2O_4$  thin film with increased Zn content was in agreement with the electrical conductivity test results (Figure 5). Figure 6(c) shows the optical transmittance spectra of  $Zn_{0.4}Cu_{0.6}Fe_2O_4$  thin films sintered in oxygen and vacuum. The transmittance decreased when sintered in oxygen. This decrease was associated with the loss of light due to an increasing number of defects such as oxygen vacancies and scattering at the grain boundaries. The transmittance spectra were converted to an  $(\alpha hv)^{1/2}$  versus  $hv$  curve as shown in Figure 6(d). The inset of Figure 6(d) shows the optical band gap of thin-film sintered in oxygen (4.770 eV) was lower compared to thin-film sintered in vacuum (4.776 eV). The decrease in optical band gap with different sintering atmosphere was in agreement with the electrical conductivity test results.



**Fig. 6.** (a) Transmittance spectra and (b) plot of  $(\alpha hv)^{1/2}$  versus  $hv$  for  $Zn_xCu_{(1-x)}Fe_2O_4$  thin films, (c) Transmittance spectra and (d) plot of  $(\alpha hv)^{1/2}$  versus  $hv$  for  $Zn_{0.6}Cu_{0.4}Fe_2O_4$  thin film sintered in oxygen and vacuum

### 3.4 Band Structure

The band structure of  $Zn_xCu_{(1-x)}Fe_2O_4$  calculated using the ABINIT program is shown in Figure 7. The calculated band gap was lower than the measured optical band gap values. For example, the calculated bandgap for  $Zn_xCu_{(1-x)}Fe_2O_4$  ( $x = 0.0$ ) was 2.205 eV compared to the measured optical band gap of 4.76 eV. This was expected because DFT calculations tend to underestimate the band gap values [23]. However, both calculated and measured band gap values increased with increasing Zn content. We compared these trends against the measured electrical conductivity (Figure 5). The calculated band structure shows that  $Zn_xCu_{1-x}Fe_2O_4$  is an indirect bandgap material with the valence band maximum (VBM) at M and conduction band minimum (CBM) at A as indicated in Figure 7. The calculated band gap of  $Zn_xCu_{1-x}Fe_2O_4$  slightly increased with increasing Zn content. The calculated band gap of  $CuFe_2O_4$  was 2.205 eV increased to 2.249 eV for  $ZnFe_2O_4$  as shown in Figure 7(a) and 7(b). The calculated band gap of  $Zn_xCu_{1-x}Fe_2O_4$  increased with increasing Zn is in agreement with the electrical conductivity test results. The calculated band gap of  $Zn_xCu_{1-x}Fe_2O_4$  with rich oxygen vacancies was slightly decreased to 2.119 eV ( $CuFe_2O_4$ ) and 2.244 eV ( $ZnFe_2O_4$ ) as shown in Figure 7(c) and 7(d). The decrease in band gap when sintered in oxygen-rich conditions was in agreement with the optical band gap and electrical conductivity test results.

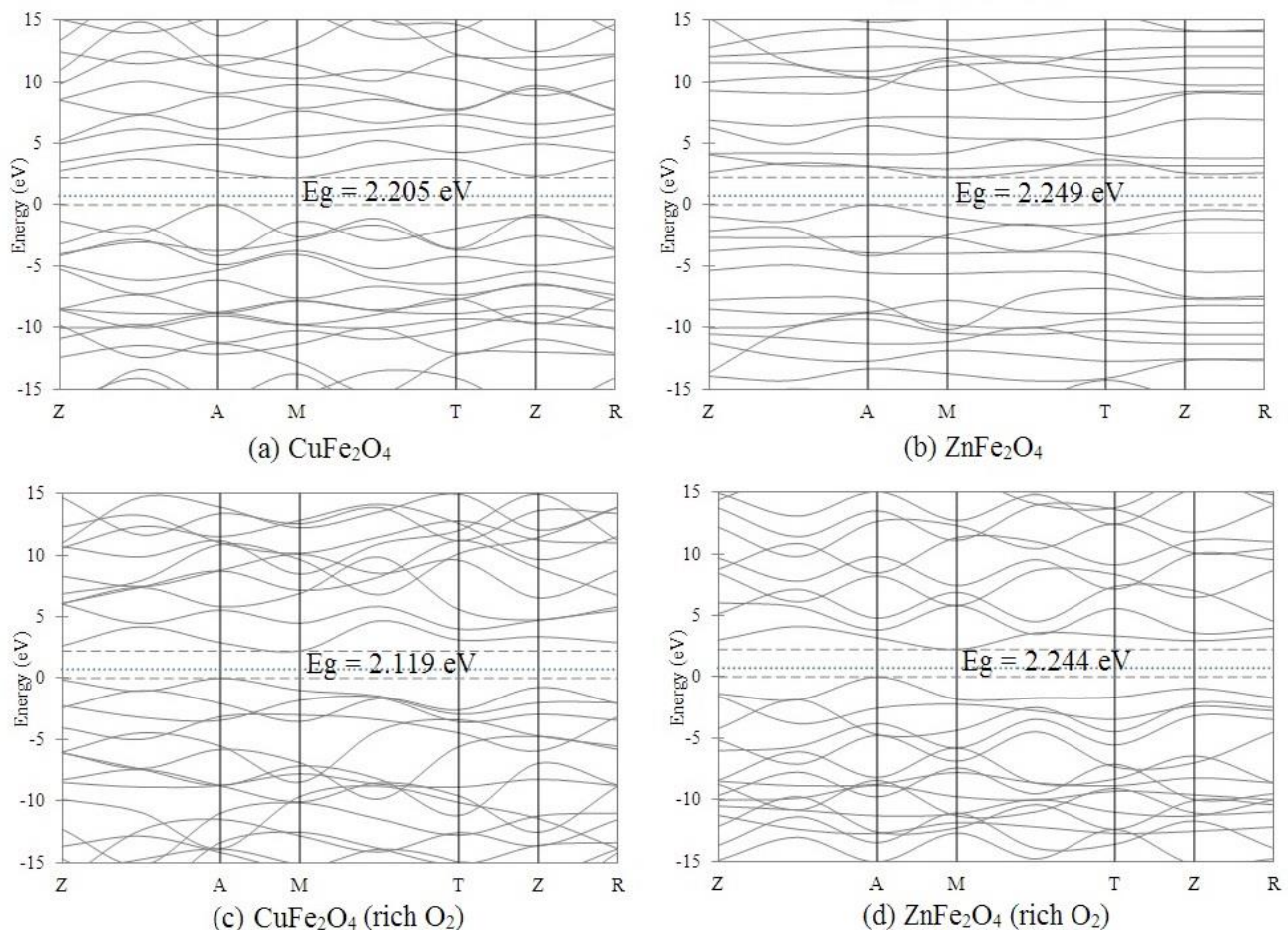


**Fig. 7.** Electronic band structure of  $Zn_xCu_{(1-x)}Fe_2O_4$

### 3.5 Thermal Analysis

The magnitude of the Seebeck coefficient for  $Zn_xCu_{(1-x)}Fe_2O_4$  thin films sintered in oxygen and vacuum are shown in Figure 8. The positive sign of the Seebeck coefficient was used to indicate the samples as p-type semiconductors and the negative sign of the Seebeck coefficient classified as n-type semiconductors. It was observed a change from n-type to p-type when  $Zn_xCu_{(1-x)}Fe_2O_4$  thin films sintered in oxygen condition. This might be due to the formation of  $Cu^+$  and  $Fe^{3+}$  brought by the presence of oxygen [21]. The observed change is consistent with values reported by other researchers [24]. The magnitude of the Seebeck coefficient for  $Zn_xCu_{(1-x)}Fe_2O_4$  thin films increased with increasing Zn content. The magnitude of Seebeck coefficient for  $Zn_xCu_{(1-x)}Fe_2O_4$  ( $x = 0.0$ ) thin films sintered in oxygen was  $6.36 \mu V/K$  which increased to  $16.72 \mu V/K$  for  $Zn_xCu_{(1-x)}Fe_2O_4$  ( $x = 1.0$ ) thin films. The presence of Zn content served to increase the Seebeck coefficient by  $10 \mu V/K$  with increasing Zn. The magnitude of the Seebeck coefficient increased concurrently with a decrease in electrical conductivity when Zn content was increased. This increasing trend was probably due to the decrease of electrical conductivity and carrier concentration [25].

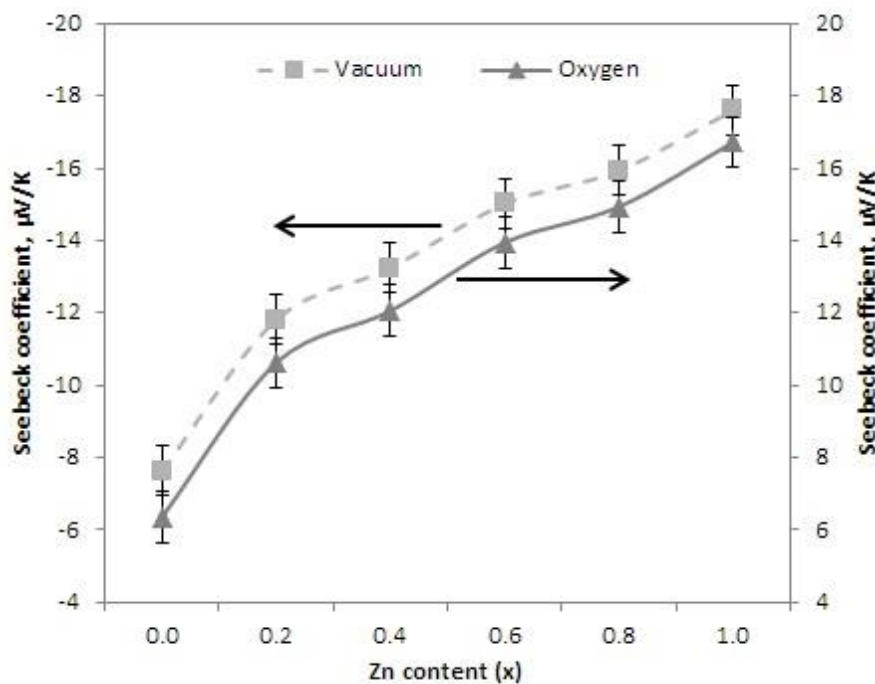


Fig. 8. Seebeck coefficient of  $Zn_xCu_{(1-x)}Fe_2O_4$  thin films

Figure 9 shows the thermal conductivity of  $Zn_xCu_{(1-x)}Fe_2O_4$  thin films sintered in oxygen and vacuum. Similar trends of test results were observed for both sintering atmospheres. The presence of Zn served to decrease thermal conductivity by  $8 W/mK$  over pure samples. The thermal conductivity of  $Zn_xCu_{(1-x)}Fe_2O_4$  ( $x = 0.0$ ) thin film was  $14.42 W/mK$  decreased to  $9.44 W/mK$  for  $Zn_xCu_{(1-x)}Fe_2O_4$  ( $x = 1.0$ ) thin film. The presence of Zn dopant served to decrease thermal conductivity over undoped samples, consistent with the increased thermal scattering potential of the larger Zn ion [26]. The thermal conductivity of the samples sintered in vacuum did not indicate a significant change compared to the samples sintered in oxygen. The sintering atmosphere did not have a significant effect on the thermal conductivity of  $Zn_xCu_{1-x}Fe_2O_4$ .

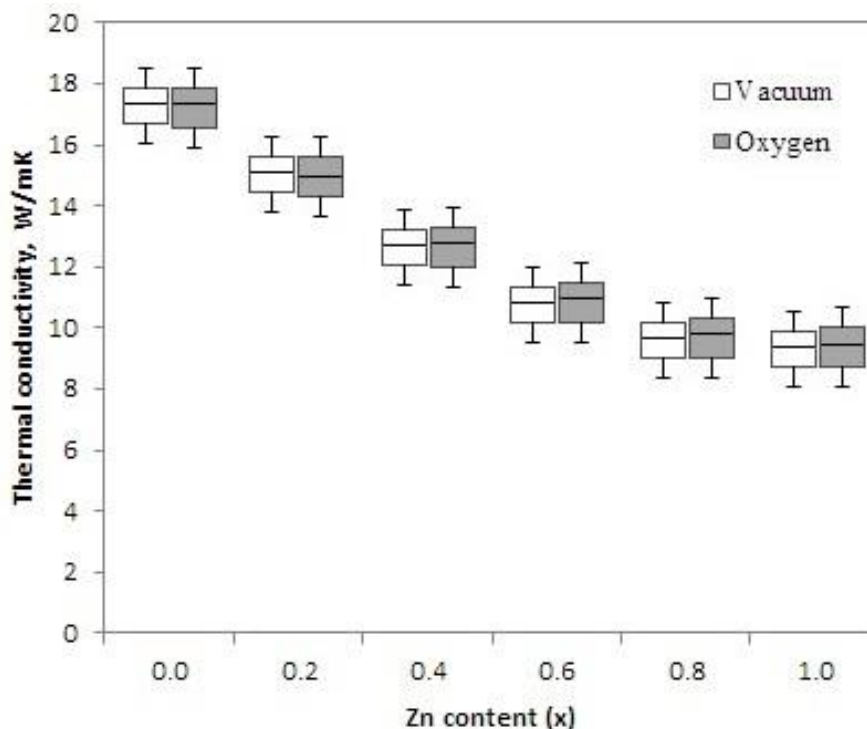


Fig. 9. Thermal conductivity of  $Zn_xCu_{(1-x)}Fe_2O_4$  thin films

#### 4. Conclusions

The  $Zn_xCu_{(1-x)}Fe_2O_4$  thin films were successfully deposited onto glass substrates using inkjet printing with a minimum of 50 print cycles to obtain homogeneous films. The XRD results show a single cubic spinel structure of Zn-Cu ferrite was obtained for thin films. The thermal and electric properties were possible to enhance by controlling the processing method sintered in oxygen and vacuum. High electrical conductivity was observed with  $Zn_xCu_{(1-x)}Fe_2O_4$  ( $x = 0.0$ ) thin-film when sintered in oxygen. The electrical conductivity of  $Zn_xCu_{(1-x)}Fe_2O_4$  sintered in oxygen was 5 % higher compared to the sample sintered in vacuum. The electrical properties were consistent with simulations based on crystal structures obtained through XRD characterization. However, the sintering atmosphere did not have a significant effect on the thermal conductivity of  $Zn_xCu_{(1-x)}Fe_2O_4$ . A lower magnitude of the Seebeck coefficient and a change in n-type to p-type of semiconductors was observed when sintered in oxygen. The magnitude of the Seebeck coefficient for  $Zn_xCu_{(1-x)}Fe_2O_4$  sintered in oxygen was about 6 % lower compared to sample sintered in vacuum due to high electrical conductivity when sintered in oxygen.

#### References

- [1] Kato, Kazuhiro, Hideo Omoto, Takao Tomioka, and Atsushi Takamatsu. "Changes in electrical and structural properties of indium oxide thin films through post-deposition annealing." *Thin Solid Films* 520, no. 1 (2011): 110-116. <https://doi.org/10.1016/j.tsf.2011.06.061>
- [2] Roncallo, S., J. D. Painter, S. A. Ritchie, M. A. Cousins, M. V. Finnis, and K. D. Rogers. "Evaluation of different deposition conditions on thin films deposited by electrostatic spray deposition using a uniformity test." *Thin Solid Films* 518, no. 17 (2010): 4821-4827. <https://doi.org/10.1016/j.tsf.2010.01.061>
- [3] Suzui, Motofumi, Shizuo Tokito, and Yasunori Taga. "Review of thin film technology in automobile industry." *Materials Science and Engineering: B* 51, no. 1-3 (1998): 66-71. [https://doi.org/10.1016/S0921-5107\(97\)00230-4](https://doi.org/10.1016/S0921-5107(97)00230-4)
- [4] Kim, H., J. S. Horwitz, S. B. Qadri, and D. B. Chrisey. "Epitaxial growth of Al-doped ZnO thin films grown by pulsed laser deposition." *Thin solid films* 420 (2002): 107-111. [https://doi.org/10.1016/S0040-6090\(02\)00658-2](https://doi.org/10.1016/S0040-6090(02)00658-2)

- [5] George, Joy. *Preparation of thin films*. CRC Press, 1992.
- [6] D.L. Smith, *Thin Film Deposition*, Mc Graw-Hill Inc, Washington D.C., 1995.
- [7] Rana, Mazhar U., Misbah-ul Islam, and Tahir Abbas. "Cation distribution and magnetic interactions in Zn-substituted CuFe<sub>2</sub>O<sub>4</sub> ferrites." *Materials chemistry and physics* 65, no. 3 (2000): 345-349. [https://doi.org/10.1016/S0254-0584\(00\)00218-2](https://doi.org/10.1016/S0254-0584(00)00218-2)
- [8] Samadashvili, I. Dzh, V. S. Varazashvili, T. E. Machaladze, and T. A. Pavlenishvili. "Thermodynamic Functions of Cu 1-x Zn x Fe 2 O 4 Ferrite Solid Solutions from 300 to 900 K." *Inorganic materials* 38, no. 11 (2002): 1186-1188. <https://doi.org/10.1023/A:1020987104575>
- [9] Darul, J., and W. Nowicki. "Preparation and neutron diffraction study of polycrystalline Cu-Zn-Fe materials." *Radiation Physics and Chemistry* 78, no. 10 (2009): S109-S111. <https://doi.org/10.1016/j.radphyschem.2009.02.009>
- [10] Duong, Binh, Supapan Seraphin, Paveena Laokul, Chivalrat Masingboon, and Santi Maensiri. "Ni-Cu-Zn ferrite prepared by Aloe vera plant extract or egg white." *Microscopy and Microanalysis* 14, no. S2 (2008): 326-327. <https://doi.org/10.1017/S1431927608083839>
- [11] Prieto, Pilar, Patricia Ruiz, Isabel J. Ferrer, Juan de la Figuera, and José F. Marco. "Nanocrystalline magnetite thin films grown by dual ion-beam sputtering." *Journal of Alloys and Compounds* 636 (2015): 150-155. <https://doi.org/10.1016/j.jallcom.2015.02.136>
- [12] Sutka, A., G. Strikis, G. Meziniskis, A. Lulis, Juris Zavickis, Jānis Kleperis, and D. Jakovlevs. "Properties of Ni-Zn ferrite thin films deposited using spray pyrolysis." *Thin Solid Films* 526 (2012): 65-69. <https://doi.org/10.1016/j.tsf.2012.11.017>
- [13] Desai, Mrugesh, Shiva Prasad, N. Venkataramani, Indradev Samajdar, A. K. Nigam, and R. Krishnan. "Annealing induced structural change in sputter deposited copper ferrite thin films and its impact on magnetic properties." *Journal of applied physics* 91, no. 4 (2002): 2220-2227. <https://doi.org/10.1063/1.1433176>
- [14] Manikandan, A., J. Judith Vijaya, L. John Kennedy, and M. Bououdina. "Structural, optical and magnetic properties of Zn<sub>1-x</sub>Cu<sub>x</sub>Fe<sub>2</sub>O<sub>4</sub> nanoparticles prepared by microwave combustion method." *Journal of molecular structure* 1035 (2013): 332-340. <https://doi.org/10.1016/j.molstruc.2012.11.007>
- [15] Stankiewicz, Jolanta, Francisco Villuendas, and Rafael Alcalá. "p-type conduction in sputtered indium oxide films." *Applied Physics Letters* 96, no. 19 (2010): 192108. <https://doi.org/10.1063/1.3430035>
- [16] Ravinder, D. "Thermoelectric power studies of zinc substituted copper ferrites." *Journal of alloys and compounds* 291, no. 1-2 (1999): 208-214. [https://doi.org/10.1016/S0925-8388\(99\)00287-X](https://doi.org/10.1016/S0925-8388(99)00287-X)
- [17] Gonze, Xavier, Bernard Amadon, P-M. Anglade, J-M. Beuken, François Bottin, Paul Boulanger, Fabien Bruneval et al. "ABINIT: First-principles approach to material and nanosystem properties." *Computer Physics Communications* 180, no. 12 (2009): 2582-2615.
- [18] Yang, Wonkyun, S. M. Rosnagel, and Junghoon Joo. "The effects of impurity and temperature for transparent conducting oxide properties of Al: ZnO deposited by dc magnetron sputtering." *Vacuum* 86, no. 10 (2012): 1452-1457. <https://doi.org/10.1016/j.vacuum.2012.02.025>
- [19] Zhang, Zhiyun, Chonggao Bao, Wenjing Yao, Shengqiang Ma, Lili Zhang, and Shuzeng Hou. "Influence of deposition temperature on the crystallinity of Al-doped ZnO thin films at glass substrates prepared by RF magnetron sputtering method." *Superlattices and Microstructures* 49, no. 6 (2011): 644-653. <https://doi.org/10.1016/j.spmi.2011.04.002>
- [20] Ajmal, Muhammad, and Asghari Maqsood. "Structural, electrical and magnetic properties of Cu<sub>1-x</sub>Zn<sub>x</sub>Fe<sub>2</sub>O<sub>4</sub> ferrites (0 ≤ x ≤ 1)." *Journal of alloys and compounds* 460, no. 1-2 (2008): 54-59. <https://doi.org/10.1016/j.jallcom.2007.06.019>
- [21] Maria, Kazi Haniun, Shamima Choudhury, and Mohammad Abdul Hakim. "Structural phase transformation and hysteresis behavior of Cu-Zn ferrites." *International Nano Letters* 3, no. 1 (2013): 42. <https://doi.org/10.1186/2228-5326-3-42>
- [22] Wang, Xinqing, Lin Chen, Qingbo Fan, Jiangxia Fan, Guangliang Xu, Minhao Yan, Mark J. Henderson, Jeremie Courtois, and Kun Xiong. "Lactoferrin-assisted synthesis of zinc ferrite nanocrystal: Its magnetic performance and photocatalytic activity." *Journal of Alloys and Compounds* 652 (2015): 132-138. <https://doi.org/10.1016/j.jallcom.2015.08.228>
- [23] Yang, Ping, Yanfang Zhao, and Haiying Yang. "Investigation on optoelectronic performances of Al, N codoped ZnO: First-principles method." *Ceramics International* 41, no. 2 (2015): 2446-2452. <https://doi.org/10.1016/j.ceramint.2014.10.059>
- [24] Stankiewicz, Jolanta, Francisco Villuendas, and Rafael Alcalá. "p-type conduction in sputtered indium oxide films." *Applied Physics Letters* 96, no. 19 (2010): 192108. <https://doi.org/10.1063/1.3430035>
- [25] Verma, Kavita, Ashwini Kumar, and Dinesh Varshney. "Effect of Zn and Mg doping on structural, dielectric and magnetic properties of tetragonal CuFe<sub>2</sub>O<sub>4</sub>." *Current Applied Physics* 13, no. 3 (2013): 467-473. <https://doi.org/10.1016/j.cap.2012.09.015>

- 
- [26] Asenath-Smith, Emily, Scott T. Misture, and Doreen D. Edwards. "Structural behavior and thermoelectric properties of the brownmillerite system  $\text{Ca}_2(\text{Zn}_x\text{Fe}_{2-x})\text{O}_5$ ." *Journal of Solid State Chemistry* 184, no. 8 (2011): 2167-2177.  
<https://doi.org/10.1016/j.jssc.2011.06.009>